Structural Characterization of a Thiazoline-Containing Chromophore in an Orange Fluorescent Protein, Monomeric Kusabira Orange[†,‡]

Akihiro Kikuchi,*[,§] Eiko Fukumura,[§,||] Satoshi Karasawa,[⊥,@] Hideaki Mizuno,[⊥] Atsushi Miyawaki,[⊥] and Yoshitsugu Shiro[§]

Biometal Science Laboratory, RIKEN SPring-8 Center, 1-1-1, Kouto, Sayo, Hyogo 679-5148, Japan, Department of Life Science, Graduate School of Science, Himeji Institute of Technology/University of Hyogo, 3-2-1, Kouto, Kamigori, Ako, Hyogo 678-1297, Japan, Laboratory for Cell Function and Dynamics, Advanced Technology Development Group, Brain Science Institute, RIKEN, 2-1, Hirosawa, Wako, Saitama 351-0198, Japan, Amalgaam Company Ltd., 2-9-3 Itabashi, Itabashi-ku, Tokyo 173-0004, Japan, and Medical and Biological Laboratories Company Ltd., 3-5-10 Marunouchi, Naka-ku, Nagoya, Aichi 460-0002, Japan

Received April 23, 2008; Revised Manuscript Received August 21, 2008

ABSTRACT: Monomeric Kusabira Orange (mKO) is a green fluorescent protein (GFP)-like protein that emits orange light at a peak of 559 nm. We analyzed its X-ray structure at 1.65 Å and found a novel three-ring chromophore that developed autocatalytically from a Cys65-Tyr66-Glu67 tripeptide in which the side chain of Cys65 formed the third 2-hydroxy-3-thiazoline ring. As a result, the chromophore contained the C═NCOH group at the 2-position of the imidazolinone moiety such that the conjugated π-electron system of the chromophore was more extended than that of GFP but less extended than that of the *Discosoma* sp. red fluorescent protein (DsRed). Since a sulfur atom has potent nucleophilic character, the third 3-thiazoline ring is rapidly and completely cyclized. Furthermore, our structure reveals the presence of a $\pi-\pi$ stacking interaction between His197 and the chromophore as well as a $\pi-$cation interaction between Arg69 and the chromophore. These structural findings are sufficient to account for the orange emission, pH tolerance, and photostability of mKO.

Aequorea victoria green fluorescent protein (GFP)[1] and GFP-like proteins from animals mainly within the class Anthozoa are useful tools in the fields of molecular and cellular biology. The number of available colors has greatly increased with the production of mutants and the discovery of new GFP-like proteins (*1*−*6*).

Although the overall folding in the case of the GFP-like proteins is identical, color variation can occur due to the structure of the chromophore, which is autocatalytically formed from the internal tripeptide. In the case of GFP from *Aequorea*, this is achieved by cyclization of the protein backbone of the Ser65-Tyr66-Gly67 sequence, leading to the formation of the 4-(*p*-hydroxybenzylidene)imidazolinone moiety (*7, 8*) (Figure 1A). The chromophore can also undergo further modification, as in the case of red-emitting *Discosoma* sp. red fluorescent protein (DsRed) in which the Gln66-Tyr67-Gly68 tripeptide autocatalytically undergoes additional oxidation at the Cα−N bond of Gln66 during the maturation process, forming C═N−C═O (acylimine) at position 2 of the imidazolinone (*9*) (Figure 1B). The crystal structure of the yellow fluorescent protein from *Zoanthus* sp., zFP538, shows a three-ring chromophore derived from

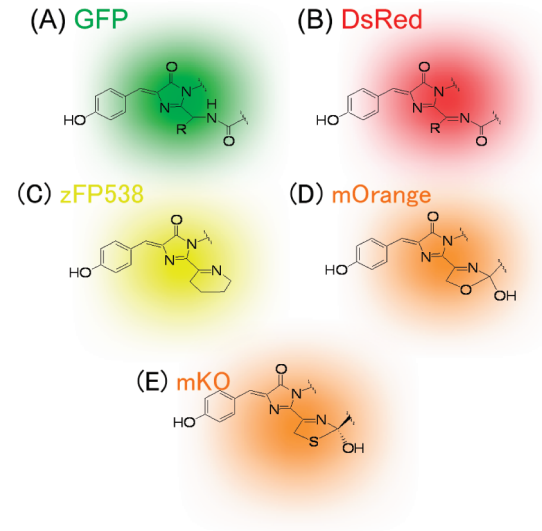

FIGURE 1: Chemical structures of the chromophore: (A) GFP, (B) DsRed, (C) zFP538, (D) mOrange, and (E) mKO.

[†] This work was supported by grants from the Molecular Ensemble Program at RIKEN.

[‡] The atomic coordinates and structural factors have been deposited in the Protein Data Bank (entry 2ZMU for mKO at pH 9.1 and entry 2ZMW for mKO at pH 6.0).

* To whom correspondence should be addressed. Phone: +81-791-58-2817. Fax: +81-791-58-2818. E-mail: kikuchi@spring8.or.jp.

[§] RIKEN SPring-8 Center.

[||] Himeji Institute of Technology/University of Hyogo.

[⊥] Brain Science Institute, RIKEN.

[@] Amalgaam Co. Ltd. and Medical and Biological Laboratories Co. Ltd.

[1] Abbreviations: GFP, green fluorescent protein; KO, Kusabira Orange fluorescent protein; mKO, monomeric KO; FRET, fluorescence resonance energy transfer; ESI-MS, electrospray ionization mass spectrometry; TFA, tetrafluoroacetate; TOF, time-of-flight; PEG, polyethylene glycol; CHES, 2-(*N*-cyclohexylamino)ethanesulfonic acid; MES, 2-(*N*-morpholino)ethanesulfonic acid; CSD, Cambridge Structural Database; rms, root-mean-square; SDS−PAGE, sodium dodecyl sulfate−polyacrylamide gel electrophoresis.

10.1021/bi800727v CCC: $40.75 © 2008 American Chemical Society
Published on Web 10/10/2008

Table 1: Comparison of Spectral Properties of Orange-Emitting Proteins

protein	absorption/ emission maximum (nm)	molar absorption coefficient (M^{-1} cm^{-1})	quantum yield	pK_a	ref
mKO	548/559	51600	0.60	~5.0	*12*
Arg69Lys[a]	564/583	3500	<0.1	ND	this work
Glu211Ala[a]	561/576	1500	0.31	ND	this work
Glu211Gln[a]	558/571	900	0.26	ND	this work
mOrange	548/562	71000	0.69	6.5	*11*

[a] The red-emitting mutants of mKO. The values of absorption maximum and molar absorption coefficient are shown only for the longest wave peak. The overall spectra are shown in Figure S4 of the Supporting Information. The values of pK_a were not determined.

the DsRed-like chromophore, which undergoes cleavage of the polypeptide backbone (*10*) (Figure 1C). Such unprecedented modification is also apparent in the crystal structure of mOrange, which is a second-generation monomeric orange fluorescent protein that has absorption and emission at 548 and 562 nm, respectively (Table 1). Its crystal structure revealed a probable heterocyclic 2-hydroxydihydrooxazole as a third ring (Figure 1D); however, detailed analysis might be complicated because of the presence of a small proportion of the immature chromophore in the final structure (*11*).

Although the details of the catalytic steps of chromophore formation remain unclear, differences in post-translational modifications of the GFP-like protein chromophore arise from variations in chromophore-forming tripeptides and noncovalent interactions between the chromophore and its immediate environment. Understanding this process will require more information about the three-dimensional structures of the GFP-like proteins than is currently available. High-resolution X-ray crystallographic studies will be important in the future for revealing such features.

The orange-emitting fluorescent protein Kusabira Orange (KO) has recently been isolated from the stony coral *Fungia concinna* (*12*). Its monomeric version, mKO, displays a sharp emission spectrum (<30 nm of the full width at half-maximum) with a maximum at 559 nm that can cover the gap in the emission spectra between green-emitting and red-emitting proteins (Table 1). It is therefore particularly useful for in vivo multicolor imaging and is one of the most desirable acceptors for fluorescence resonance energy transfer (FRET) measurements due to its high light-absorbing capability with low pH sensitivity and high photostability. More recently, a new variant of mKO has successfully been used to construct cell cycle fluorescent probes named "Fucci" (the fluorescent ubiquitination-based cell cycle indicator) (*13*).

Here, we present the crystal structure of mKO (pH 9.1) at a resolution of 1.65 Å. This high-resolution structure revealed that mKO contains a fully mature chromophore containing a 3-thiazoline ring as a third ring. In addition, we confirmed the identical chromophore in the crystal structure crystallized at pH 6.0 (2.0 Å resolution). The three-ring chromophore accounts for the orange-emitting ability of the protein. On the basis of the analysis of the chromophore and its immediate environment as well as a mutagenesis study, we propose a model for the formation of the third ring structure.

EXPERIMENTAL PROCEDURES

Materials and Methods. The mKO variants were generated by site-directed mutagenesis. The proteins were expressed in *Escherichia coli*, purified, and characterized spectroscopically as previously described (*12*). The mKO proteins were concentrated to approximately 10 mg/mL in 20 mM Tris-HCl (pH 8) for crystallization.

Electrospray Ionization Mass Spectrometry Analysis. The protein solution was acidified by adding 4 volumes of water containing 0.1% tetrafluoroacetate (TFA) and absorbed on ZipTipC18 (Millipore, Billerica, MA). The sample on the tip was washed with 100 μL of a 5% acetonitrile/0.1% TFA solution in water and eluted with 5 μL of an 80% acetonitrile/0.1% TFA solution in water. The eluate was packed into precoated borosilicate nanoelectrospray needles (EconoTip; New Objective, Woburn, MA), and the protein was ionized by direct nanoelectrospray infusion at a capillary voltage of 1.5 kV (MDS Proteomics). The mass spectrum was acquired with a QSTAR Hybrid quadrupole time-of-flight (TOF) mass spectrometer (Applied Biosystems/MDS Sciex). The mass range was set to *m/z* 350−1700. Data were analyzed with Analyst QS (Applied Biosystems/MDS Sciex).

Crystallization. mKO was crystallized by the hanging drop vapor diffusion method at room temperature. The following two different forms were obtained: hexagonal crystals that were produced at room temperature in 50% polyethylene glycol (PEG) 200 and 0.1 M 2-(*N*-cyclohexylamino)ethanesulfonic acid (CHES) (pH 9.1) over a period of 2−3 days and monoclinic crystals that grew in 30% PEG 200, 5% PEG 3000, and 0.1 M 2-(*N*-morpholino)ethanesulfonic acid (MES) (pH 6.0), which reached a maximum size of 0.3 mm × 0.4 mm × 0.2 mm after 4−5 days.

X-ray Structure Analysis. All data sets were collected at 100 K using synchrotron radiation at SPring-8 on RIKEN beamline BL44B2 with a wavelength of 1.0 Å. The data sets were indexed and reduced with the HKL2000 package (*14*). The structure of mKO at pH 9.1 was determined by molecular replacement with Molrep (*15*) in the CCP4 suite using the monomer from the Rtms5 structure [Protein Data Bank (PDB) entry 1MOU] (*16*) as the starting model, with the chromophore deleted. The obtained electron density map was clear, allowing most of the amino acid sequence to be automatically traced using ARP/wARP (*17*). Although automatic modeling of the chromophore was not completely successful, dummy atoms appearing in the ARP/wARP cycles indicated a covalent bond between Sγ of Cys65 and the carbonyl carbon of Phe64, leading to the formation of an additional thioamide ring.

On the basis of the autotraced model, the final model was manually constructed using TURBO-FRODO (*18*), and refinement was carried out with CNS (*19*). Different restrained parameters for the chromophore were tested to determine the best fit to the electron density map. Although the bond between the chromophore and Phe64 was initially unrestrained, the model was never fit into the electron density. Thus, the Phe64 residue was considered to be a fraction of the chromophore in the restrained parameter. The restrained parameter for the chromophore in which the Sγ−C* distance is 1.83 Å and the Cβ−Sγ−C* angle is 89.3° (atom labeling shown in Figure 3) is within the range prescribed for the thiazoline structures found in the Cam-

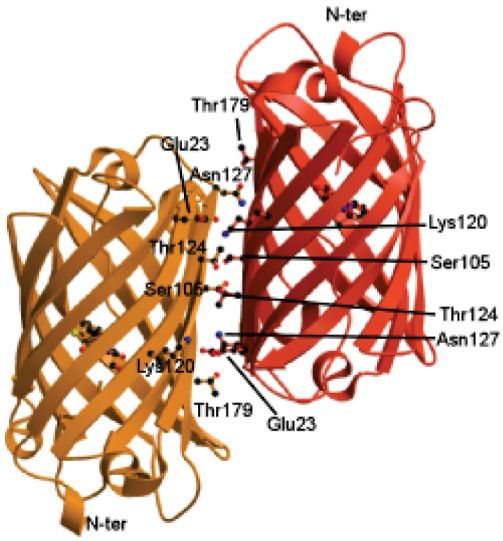

FIGURE 2: Ribbon diagram of the overall mKO dimer structure in the $P3_121$ crystal form. Residues of the dimer interface and chromophores are represented as a ball-and-stick model.

bridge Structural Database (CSD) (*20*); this led to the best fit of the chromophore to the electron density map. Although the Cα−N−C* bond angle (122°) in the restrained parameter appeared to deviate slightly from that of the range of thiazoline structures found in the CSD, the value was very similar to that of the model autotraced with ARP/wARP. The overall R and R_{free} values finally converged to 0.205 and 0.207, respectively.

The structure of the monoclinic $P2_1$ crystal grown at pH 6.0 was determined by molecular replacement using the mKO structure at pH 9.1 as the starting model. Refinement was carried out with CNS without the application of noncrystallographic symmetric restraints. The final model had an R factor of 0.197 and an R_{free} of 0.231 for all reflections between 20 and 2.0 Å.

RESULTS

Overall Structure of mKO. The mKO crystals grown at pH 9.1 were characterized as belonging to hexagonal space group $P3_121$. Diffraction data were observed to a maximum resolution of 1.65 Å, with the following unit cell parameters: $a = b = 97.90$ Å and $c = 89.83$ Å. One mKO molecule was contained within the asymmetric unit, although the V_m value was calculated as 4.86 Å^3/Da with a solvent content of 74.7%. The crystals obtained at pH 6.0 were found to be in monoclinic space group $P2_1$ with four mKO molecules in the asymmetric unit ($V_m = 2.88$ Å^3/Da) and the following unit cell parameters: $a = 92.57$ Å, $b = 72.11$ Å, $c = 90.27$ Å, and $\beta = 102.72°$.

We determined the crystal structures of mKO for both crystal forms (Table 2). The model contained residues 2−218 and exhibited excellent stereochemistry. It had an R factor of 0.205 and an R_{free} of 0.207 at a resolution of 1.65 Å. Structural evaluations of the final models using PROCHECK (*21*) indicated that 94.9% of the residues were in the most favorable regions of the Ramachandran plot, with no residues in the disallowed regions. The overall structures of mKO were similar to those of GFP and GFP-like proteins (Figure 2), an 11-stranded β-barrel with a coaxial central α-helix holding a chromophore (so-called "β-can fold") (*7*−*9*). The structure of mKO grown at pH 6.0 was identical to that at pH 9.1, exhibiting a root-mean-square (rms) deviation of 0.27 Å for all Cα atoms (data not shown).

The superposition of mKO with mOrange (47% identical sequences) produced a rms deviation of 1.0 Å for 208 equivalent Cα atoms. The dimer formation of mKO was observed by crystallographic symmetry in the $P3_121$ crystal and within an asymmetric unit in the $P2_1$ form. In both structures, the dimer interface was mediated by several residues (Figure 2). The mode of the dimer interface, however, was quite different from the typical dimer found in the DsRed structure (*9*), in which the dimer interface involves carboxy termini. The dimer structure of mKO is rather artificial and may be insignificant in terms of its promise as an in vivo marker.

Novel Three-Ring Chromophore. The most striking feature of mKO was its chromophore structure, which was well-characterized in the high-quality electron density map at a resolution of 1.65 Å (Figure 3). The cis-coplanar chromophore in mKO was formed from the internal Cys65-Tyr66-Gly67 tripeptide, in which Cys65 apparently participated in the formation of the additional 2-hydroxy-3-thiazoline ring. Thus, the chromophore of mKO contained a phenolate ring, imidazolinone, and a third 3-thiazoline ring. The Cβ(Cys65)−Sγ(Cys65)−C*(carbonyl carbon of Phe64) angle and the bond distance between the Sγ atom of Cys65 and C* of Phe64 were 89° and 1.83 Å, respectively. The torsion angle of the Cα−N and Sγ−C* bonds was 11°, suggesting that the ring was almost flat. These observations were in accordance with the crystal structures of small molecules containing 3-thiazoline moieties found in the CSD.

The 3-thiazoline ring was twisted out of plane by only 6.7° from the 4-(*p*-hydroxybenzylidene)-5-imidazolinone moiety, indicating that both rings were nearly coplanar (Figure 3). This feature was consistent with the fact that the α-carbon of Cys65 exhibited an sp^2 hybrid conformation, accounting for the double bond character of the Cα=N group in Cys65. In contrast, C* of Phe64 appeared to exhibit tetrahedral geometry (sp^3 hybridization), indicating formation of a Cα=N−C*(Phe64)−OH moiety. Thus, we concluded that the structure of the mKO chromophore (Figure 1E) comprised three rings, similar to that of mOrange, which contains a dihydrooxazole ring as the third ring (Figure 1D).

The formation of the three-ring mKO chromophore was confirmed by mass spectroscopy. The electrospray ionization mass spectrometry (ESI-MS) spectrum indicated a molecular mass of 25365.67 Da for mature mKO (data shown in Figure S1 of the Supporting Information), while the theoretical molecular mass of the mKO peptide chain (as calculated from its amino acid sequence) was 25387.73 Da. The 22 Da reduction upon chromophore formation can be explained in terms of cyclization (that is, loss of H_2O and 2H) and oxidation (that is, O_2-mediated loss of 2H) in the formation of the imidazolinone ring and by additional oxidation of the peptide during the formation of the 3-thiazoline ring. Thus, the observed mass was consistent with the formation of the Cα=N−C*−OH moiety (Figures 1E and 3).

In addition, sodium dodecyl sulfate−polyacrylamide gel electrophoresis (SDS−PAGE) of preboiled mKO showed a fragment band with an apparent mass of 19 kDa; this reinforces the presence of a C=N bond in mKO (data shown in Figure S2 of the Supporting Information). It is notable

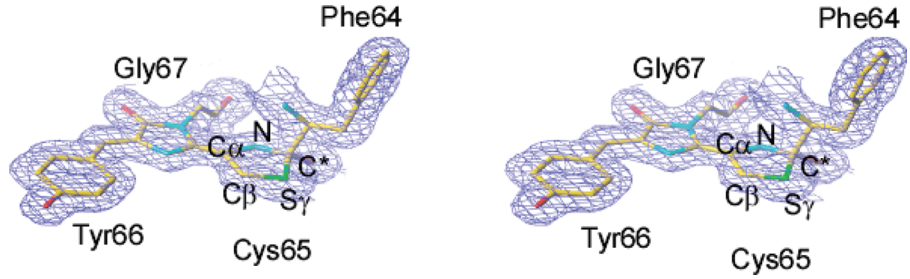

FIGURE 3: Stereoview of the final omit electron density map superimposed on the mKO chromophore. The contour level is 1.2σ.

Table 2: Crystallographic Statistics for mKO

	mKO at pH 9.1	mKO at pH 6.0
PDB entry	2ZMU	2ZMW
	Data Collection	
space group	$P3_121$	$P2_1$
unit cell		
a, b, c (Å)	97.90, 97.90, 89.83	92.57, 72.11, 90.27
α, β, γ (deg)	90, 90, 120	90, 102.7, 90
radiation source	SPring-8 BL44B2	SPring-8 BL44B2
wavelength (Å)	1.0	1.0
overall resolution (Å)	50.0−1.65	50.0−2.00
(outer shell)	(1.71−1.65)	(2.07−2.00)
no. of reflections		
measured	631752	260637
unique	59751	77722
completeness (%)	99.4 (100.0)	98.5 (98.5)
$\langle I/\sigma(I)\rangle$	69.9 (7.6)	23.1 (5.5)
R_{merge} (%)	4.9 (32.7)	7.4 (32.7)
	Refinement	
resolution range (Å)	20−1.65	20−2.0
no. of reflections used	59696	77299
R_{cryst} (%)	20.5	19.7
R_{free} (%)	20.7	23.1
no. of water atoms	263	762
rms deviation		
bond lengths (Å)	0.005	0.006
bond angles (deg)	1.40	1.35
average B factor (Å)		
protein	25.6	21.8
water	42.6	36.0
Ramachandran plot		
most favorable (%)	94.9	93.8
additionally allowed (%)	5.1	6.2

that an attempt to enhance the polypeptide fragmentation in 0.1 M HCl resulted in the absence of the SDS−PAGE band due to unpredictable fragmentation of the protein (data not shown).

Chromophore Environment. The immediate environment around the chromophore of mKO was comparable with that of mOrange (*11*) (Figure 4A,B). The Arg94 and Glu212 residues of mKO were found in a position similar to that of Arg95 and Glu215 of mOrange, respectively. These two residues are known to be well-conserved among the GFPs and GFP-like proteins. Glu212 in mKO makes contact with the buried water molecule (W1) and the positively charged side chain of Arg69 at distances of 2.6 and 3.2 Å, respectively. The Glu212−Arg69 interaction found in mKO facilitates a cyclic interaction network mediated by hydrogen bonding and charge−charge interactions via the buried water molecule (W2), Glu147, and His197 on one side of the chromophore (Figure 4B). The cyclic interaction network is further extended to the opposite side of the chromophore via Glu147, the buried water molecule (W2), and the conserved Tyr180 and Arg94 residues. The conserved Arg94 makes close contact with the imidazolinone oxygen of the chromophore in association with the water molecule (W3) (Figure 4B).

The Glu212−Arg69 interaction observed in mKO was comparable with the Glu215−Lys70 interaction in mOrange; however, the interaction was not direct. It occurred via buried water molecules (Figure 4A). Furthermore, the buried and charged residues Lys70 and Glu148 in mOrange interacted closely with the chromophore but did not participate in the cyclic interaction network as His197 in mKO was replaced with Ile197 in mOrange. This His197 residue is likely to be a key residue resulting in major structural differences in mKO compared with mOrange.

The imidazole ring of His197 in mKO was parallel to the phenol ring of the chromophore with an angle of <5° between the planes, while the plane-to-plane distance was estimated to be 3.3−3.4 Å. These geometries are representative of the $\pi-\pi$ stacking interaction in an off-centered orientation, which is energetically favorable to protein stabilizations (*22*). As His197 makes contact with Glu212 and Glu147 at a distance of approximately 3 Å, it is likely that the imidazole ring is cationic. The resulting positive charge could stabilize the anionic form of the chromophore phenolate, together with the Ser145 interaction and the nearby water molecule (W4). It is noteworthy that the substitution of His193 with Thr, Ile, Ser, or Asn has a significant effect on the fluorescent emission of mKO. Contrary to the previous study on amFP486 (*23*), the His193 mutants have no light-emitting ability (data shown in Figure S3 of the Supporting Information).

Another structural difference between mKO and mOrange was that Arg69 in mKO was positioned above the chromophore; thus, its side chain could directly interact with the chromophore (a so-called cation$-\pi$ interaction) (*24*), while the mOrange Lys70 side chain was observed to move away from the chromophore plane and interact with Glu148 and imidazolinone oxygen.

Red-Emitting Mutants of mKO. The crystal structure of mKO revealed that Glu212 and Arg69 were not only sequentially but also structurally conserved. Thus, directed mutagenesis of the residues has been used to investigate the formation mechanism of the mKO chromophore. The substitution of Glu212 with Ala or Gln resulted in red emission proteins that exhibited a peak maximum at 576 or 571 nm, respectively (Figure 5). The replacement of Arg69 with Lys also affected the emission spectrum and resulted in a red-shifted emission maximum at 583 nm. The other spectral features of the red-emitting mutants are summarized in Table 1 (the absorption spectra are shown in Figure S4 of the Supporting Information). The small value of the molar absorption coefficient suggested inefficient maturation of the chromophore, which is in accordance with the role of Glu212

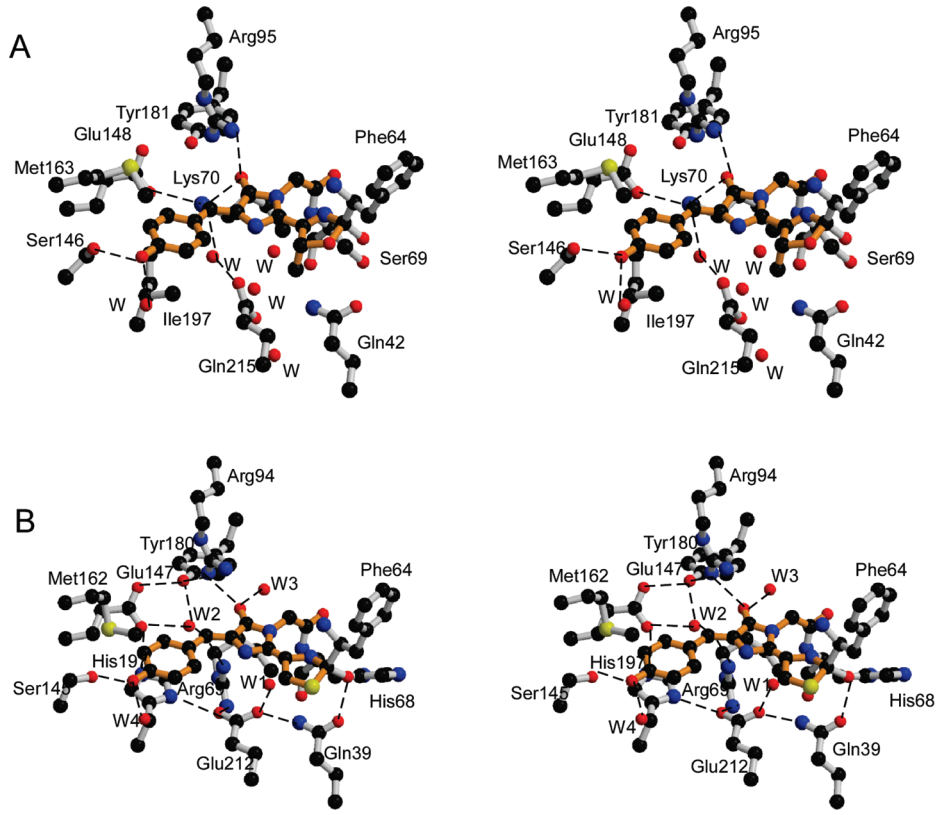

FIGURE 4: Stereoview of chromophore environments showing hydrogen bonding and charge−charge interactions (− − −) of (A) mOrange taken from PDB entry 2H5O and (B) mKO.

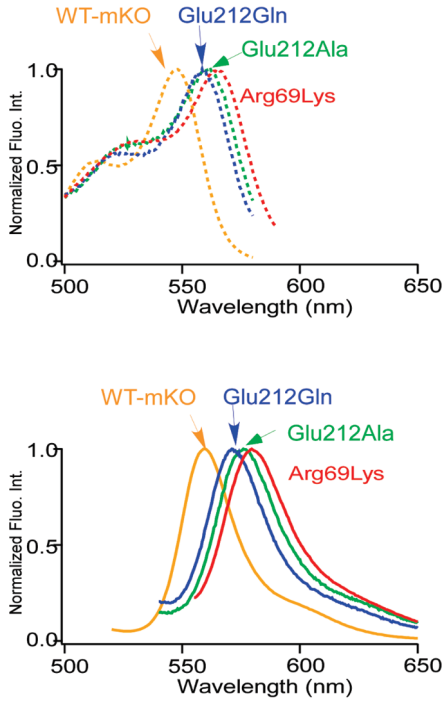

FIGURE 5: Comparison of normalized excitation (top) emission (bottom) spectra between mKO (orange) and its red-emitting mutants, Glu212Gln (blue), Glu212Ala (green), and Arg69Lys (red).

and Arg69 in the chromophore formation mechanism (*25, 26*). For example, the Arg69Lys variant significantly decreased the fluorescence quantum yields to <0.1. Furthermore, polypeptide fragmentations were observed by SDS−PAGE analysis of the preboiled full-length mutants (data shown in Figure S2 of the Supporting Information). These results indicate that the DsRed-like chromophore containing acylimine is the intermediate that produces the completely mature chromophore in the case of the untouched mKO.

DISCUSSION

Structural Basis of mKO Fluorescent Properties. The size of the delocalized chromophore π system is considered an important factor in determining the fluorescent color of GFPs and GFP-like proteins. For example, a shift to red in the spectra is caused by an increase in the size of the delocalized π system (*27, 28*). In the case of red-emitting proteins such as DsRed, the π system is more extended by additional conjugation due to the formation of the acylimine (C═N−C═O) moiety at position 2 of the imidazolinone ring (λ_{em}^{max} = 583 nm) (*9*) (Figure 1B). In green-emitting proteins such as GFP, the conjugated π system delocalizes only in the two flat aromatic rings, namely, the 4-(*p*-hydroxybenzylidene)-5-imidazolinone moiety (Figure 1A), producing an emission peak maximum at 504 nm (*5*).

The crystal structure of mKO reported here reveals that the chromophore has an additional 3-thiazoline ring, namely, a Cα═N−C−OH moiety with a 4-(*p*-hydroxybenzylidene)-5-imidazolinone group (Figure 1E). The additional Cα═N group causes an extension of the π conjugate system from the green-emitting chromophore, but the delocalized π system of the mKO chromophore is less extended than that of DsRed. Thus, the orange emitting ability of mKO (λ_{em}^{max} = 559 nm) (*12*) demonstrates a peak in the emission spectra between GFP and DsRed. This is in line with the chromophore found in the crystal structure of mOrange in which a third ring is formed upon reaction of the oxygen atom of Thr66 with the Cα atom of Phe65, resulting in the formation

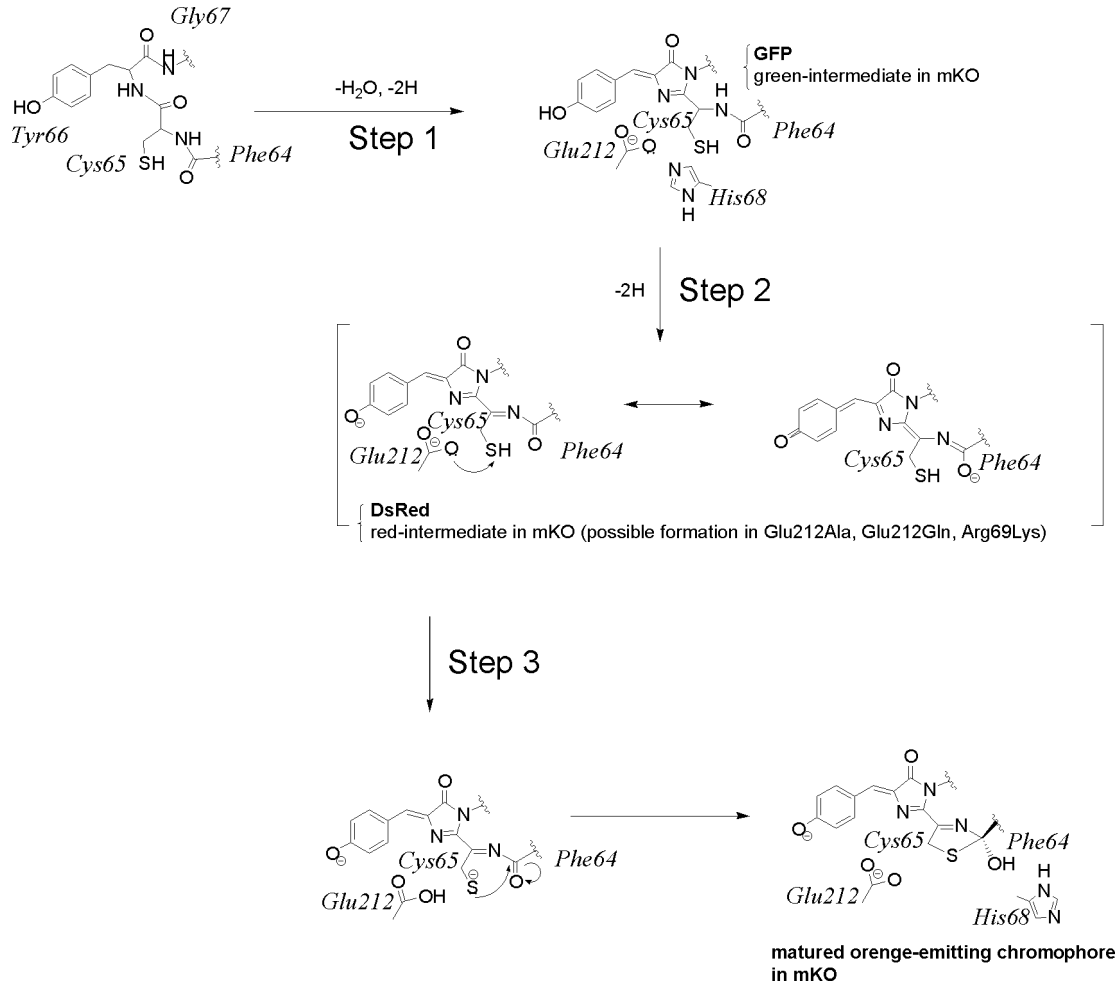

FIGURE 6: Proposed model for formation of the orange-emitting three-ring chromophore in mKO. The chromophore forms green-emitting and red-emitting acylimine intermediates in the first and second steps, respectively. Subsequently, the acylimine is attacked by the Sγ atom of Cys65 to form a new five-membered thioamide ring, representing the complete mature orange-emitting chromophore.

of a third dihydrooxazole ring (Figure 1D). In the case of mOrange, however, the structure is a mixture of the mature (three-ring) and immature (two-ring) forms (*11*). As a sulfur atom has a more potent nucleophilic character than an oxygen atom, the cyclization of the third ring in the mKO chromophore is likely to result in a completely mature structure. In fact, the observed Sγ−C* bond length in this study (1.83 Å) was in accordance with that of a normal single S−C bond (1.8 Å). Therefore, the mKO structure could be an appropriate model for understanding the structural features that control the additional autocatalytic posttranslational modification processes occurring in GFP-like proteins.

Proposed Formation of the Chromophore. As shown in Figure 6, we propose that the mKO chromophore matures in a three-step process. The first step is the formation of 4-(*p*-hydroxybenzylidene)-5-imidazolinone, similar to the formation of the GFP chromophore. Indeed, the green fluorescent intermediate can be observed transiently in the chromophore maturation process of tetrameric KO, which is the precursor of mKO (*12*). The second step is the formation of the red-emitting acylimine intermediate, similar to DsRed. Although the putative intermediate has never been observed, some mKO mutants, Glu212Ala, Glu212Gln, and Arg69Lys, exhibit red fluorescence instead of orange (Figure 5). The DsRed-like red-emitting chromophore is suspected to be the putative intermediate in the mutants. The third and final step is the nucleophilic attack by the Sγ atom of Cys65 on the acylimine moiety of the chromophore in the former intermediate which forms a new five-membered 3-thiazoline ring.

In this formation, abstraction of a proton from the Cys65-SH group is likely to be an important step in the additional cyclization required to produce the third 3-thiazoline ring. The deprotonation would be catalyzed or promoted by the Glu212 residue, which is possibly present in an anionic form, via the cyclic interaction network formed by Arg69, Glu147, His197, Glu212, and a water molecule (W2) (Figure 4B). The network would favor the basic character of Glu212 carboxylate, promoting the deprotonation of the Cys65-SH group. The significance of the anionic character of Glu212 in proton abstraction from the Cys65-SH group was supported by our mutation results. Mutation of Glu212 to Ala or Gln converted mKO into a red-emitting protein with emission peak maxima at 576 and 571 nm, respectively (Figure 5), and resulted in inefficient maturation of the chromophore. As the Ala and Gln residues are not capable of abstracting a proton from Cys65, the third maturation step would be excluded in the mutants, resulting in a red-emitting chromophore (Figure 6).

Substitution of Arg69 with Lys also resulted in a red-emitting protein ($\lambda_{em}^{max} = 582$ nm) with spectral characteristics similar to those of DsRed ($\lambda_{em}^{max} = 583$ nm) (Figure 5). The quantum yield of the fluorescence consequently

decreased (<0.1), indicating that Arg69 plays a pivotal role in the final step of formation of the orange-emitting chromophore. We superimposed the DsRed structure (PDB entry 1G7K) on mKO. This demonstrated that the Lys residue in DsRed occupied a position similar to that of Arg69 in the mKO structure. However, the side chain of Lys70 was positioned directly on the imidazole ring of His197, resulting in the obstruction of the space around the substituted Lys residue by steric hindrance (data not shown). Thus, Lys69 in the Arg69Lys mutant is unable to occupy an appropriate position for making contact with Glu212 and can no longer maintain the basicity of its carboxylate to enable deprotonation of thiole. This would arrest chromophore maturation of the mutant in the final step, resulting in the formation of the red-emitting chromophore. The Lys residue has a positive charge identical to that of Arg, and significant movement caused by the substitution of Arg with Lys would not be expected. Nevertheless, this is a reasonable explanation for the difference between mKO and its red-emitting mutant because it has been reported that such weak interactions between residues with anion and aromatic side chains (or extended π system chromophores) play important roles in the spectroscopic properties of GFP-like proteins (*27*).

pH Tolerance and Photostability of mKO. mKO exhibits low pH sensitivity, i.e., pH tolerance of the molar absorption coefficient (apparent pK_a = 5.0), making it an ideal FRET acceptor (*12*). The fact that all residues and buried water molecules found in mKO at pH 6.0 ($P2_1$ form) were perfectly interspaced at a position identical to that in mKO at pH 9.1 ($P3_121$ form) is consistent with the low sensitivity (data shown in Figure S5 of the Supporting Information). With respect to the GFP-based techniques, proteins with simple spectra are preferable, and the anionic character of the chromophore (phenolate) is considered to be more important for the detection of fluorescence than the neutral form. In the case of DsRed, the charge−charge interaction with Lys163 maintains the anionic charge of the chromophore Tyr67 phenol (apparent pK_a = 4.7) (*9*). The Lys163 residue is replaced with Met162 in mKO, but the imidazole group of His197 possibly has a cationic character due to the cyclic interaction network (Glu212, Arg69, H_2O, and Glu147). Therefore, the stacking effect caused by the His197 imidazole should contribute to the stabilization of the anionic form of the chromophore in mKO. In contrast, the pK_a value of mOrange (6.5) is estimated to be higher than that of mKO (Table 1), probably because of the replacement of His193 with Ile197. Similar structural characteristics have been discussed in other GFP-like proteins, such as zFP538 and amFP486, in which the pK_a values are estimated to be lower than that of mOrange (*10, 23*).

The $\pi-\pi$ stacking between the His197 imidazole ring and the chromophore phenol ring in mKO could also contribute to stabilization of the anionic state of the chromophore as well as its planarity. This is an important factor for the brightness of the protein, which is derived from the quantum yield and molar extinction. This observation has also been made for amFP486 (*23*). The chromophore of its His199Thr mutant in which the $\pi-\pi$ stacking interaction is absent adopted a trans as well as a cis conformation, resulting in extensive loss of brightness. The His193 residue is replaced with Ile197 in mOrange, resulting in a ruin of retentive support for maintaining the planarity and/or phenolic character of the chromophore. Moreover, the cation$-\pi$ interactions between the π electron system, such as the aromatic ring, and adjacent cations are noncovalent molecular interactions that are sufficiently strong to stabilize proteins and/or protein−ligand complexes (*24*). Therefore, the presence of the cation$-\pi$ interaction between Arg69 and the chromophore of mKO is in accordance with its higher photostability compared with that of mOrange. In the latter structure, Lys70 moves away from the chromophore plane and would be less likely to participate in a cation$-\pi$ interaction.

Therefore, we propose that a combination of noncovalent bonds between the surrounding residues, such as His193 and Arg69, and the chromophore contributes to the low pH sensitivity and high photostability of the mKO protein. The structural comparison between mKO and mOrange (Figure 4A,B) and the fact that the His193 mutants of mKO yielded proteins with no fluorescence strengthen our proposal.

CONCLUSIONS

In summary, we propose that the orange emitting property of mKO arises from its novel three-ring chromophore consisting of the phenolate ring, the imidazolinone, and the 3-thiazoline ring. The extension of the conjugated π electron system of the chromophore could reasonably explain the orange fluorescence of mKO. Noncovalent bonding interactions between the chromophore and His197 ($\pi-\pi$ stacking interaction) and Arg69 (cation$-\pi$ interaction) also favor orange emission with low pH sensitivity and high brightness. The acylimine chromophore appears to act as an intermediate for further autocatalytic posttranslational modification in the maturation process of GFP-like proteins. It will thus be of considerable interest to find additional GFP-like proteins with novel chromophores to provide further insight into the posttranslational modification of proteins.

ACKNOWLEDGMENT

We thank Dr. Kaori Otsuki and Dr. Masaya Usui (Brain Science Institute Research Resources Center in RIKEN, 1-1-1, Wako, Saitama, Japan) for the mass spectral analysis.

SUPPORTING INFORMATION AVAILABLE

ESI-MS of mKO (Figure S1), SDS−PAGE of mKO and the red-emitting mutants (Figure S2), colonies of *E. coli* expressing mKO and the His193 mutants (Figure S3), absorption spectra of the red-emitting mutants (Figure S4), and comparison of the chromophore environment of mKO structures between pH 6.0 and 9.1 (Figure S5). This material is available free of charge via the Internet at http://pubs.acs.org.

REFERENCES

1. Labas, Y. A., Gurskaya, N. G., Yanushevich, Y. G., Fradkov, A. F., Lukyanov, K. A., Lukyanov, S. A., and Matz, M. V. (2002) Diversity and evolution of the green fluorescent protein family. *Proc. Natl. Acad. Sci. U.S.A. 99*, 4256–4261.
2. Matz, M. V., Fradkov, A. F., Labas, Y. A., Savitsky, A. P., Zaraisky, A. G., Markelov, M. L., and Lukyanov, S. A. (1999) Fluorescent proteins from nonbioluminescent anthozoa species. *Nat. Biotechnol. 17*, 969–973.
3. Miyawaki, A., Sawano, A., and Kogure, T. (2003) Lighting up cells: Labelling proteins with fluorophores. *Nat. Cell Biol. 5* (Suppl.), S1−S7.

4. Shaner, N. C., Steinbach, P. A., and Tsien, R. Y. (2005) A guide to choosing fluorescent proteins. *Nat. Methods 2*, 905–909.
5. Tsien, R. Y. (1998) The green fluorescent protein. *Annu. Rev. Biochem. 67*, 509–544.
6. Zhang, J., Campbell, R. E., Ting, A. Y., and Tsien, R. Y. (2002) Creating new fluorescent probes for cell biology. *Nat. Rev. Mol. Cell Biol. 3*, 906–918.
7. Ormö, M., Cubitt, A. B., Kallio, K., Gross, L. A., Tsien, R. Y., and Remington, S. J. (1996) Crystal structure of the *Aequorea victoria* green fluorescent protein. *Science 273*, 1392–1395.
8. Yang, F., Moss, L. G., and Phillips, G. N., Jr. (1996) The molecular structure of green fluorescent protein. *Nat. Biotechnol. 14*, 1246–1251.
9. Yarbrough, D., Wachter, R. M., Kallio, K., Matz, M. V., and Remington, S. J. (2001) Refined crystal structure of DsRed, a red fluorescent protein from coral, at 2.0-Å resolution. *Proc. Natl. Acad. Sci. U.S.A. 98*, 462–467.
10. Remington, S. J., Wachter, R. M., Yarbrough, D. K., Branchaud, B., Anderson, D. C., Kallio, K., and Lukyanov, K. A. (2005) zFP538, a yellow-fluorescent protein from *Zoanthus*, contains a novel three-ring chromophore. *Biochemistry 44*, 202–222.
11. Shu, X., Shaner, N. C., Yarbrough, C. A., Tsien, R. Y., and Remington, S. J. (2006) Novel chromophores and buried charges control color in fruits. *Biochemistry 45*, 9639–9647.
12. Karasawa, S., Araki, T., Nagai, T., Mizuno, H., and Miyawaki, A. (2004) Cyan-emitting and orange-emitting fluorescent proteins as a donor/acceptor pair for fluorescence resonance energy transfer. *Biochem. J. 381*, 307–312.
13. Sakaue-Sawano, A., Kurokawa, H., Morimura, T., Hanyu, A., Hama, H., Osawa, H., Kashiwagi, S., Fukami, K., Miyata, T., Miyoshi, H., Imamura, T., Ogawa, M., Masai, H., and Miyawaki, A. (2008) Visualizing spatiotemporal dynamics of multicellular cell-cycle progression. *Cell 132*, 487–498.
14. Otwinowski, Z., and Minor, W. (1997) Processing of X-ray diffraction data collected in oscillation mode. *Methods Enzymol. 276*, 307–326.
15. Vagin, A. A., and Isupov, M. N. (2001) Spherically averaged phased translation function and its application to the search for molecules and fragments in electron-density maps. *Acta Crystallogr. D57*, 1451–1456.
16. Prescott, M., Ling, M., Beddoe, T., Oakley, A. J., Dove, S., Hoegh-Guldberg, O., Devenish, R. J., and Rossjohn, J. (2003) The 2.2 Å crystal structure of a pocilloporin pigment reveals a nonplanar chromophore conformation. *Structure 11*, 275–284.
17. Lamzin, V. S., Perrakis, A., and Wilson, K. S. (2001) The ARP/WARP suite for automated construction and refinement of protein models In *International Tables for Crystallography. Vol. F: Crystallography of biological macromolecules* (Rossmann, M. G., and Arnold, E., Eds.) pp 720−722, Kluwer Academic Publishers, Dordrecht, The Netherlands.
18. Roussel, A., and Cambillau, C. (1989) TURBO-FRODE. In *Silicon Graphics Geometry Partner Directory*, pp 77−78, Silicon Graphics, Mountain View, CA.
19. Brünger, A. T., Adams, P. D., Clore, G. M., DeLano, W. L., Gros, P., Grosse-Kunstleve, R. W., Jiang, J. S., Kuszewski, J., Nilges, M., Pannu, N. S., Read, R. J., Rice, L. M., Simonson, T., and Warren, G. L. (1998) Crystallography and NMR System: A new software suite for macromolecular structure determination. *Acta Crystallogr. D54*, 905–921.
20. Allen, F. H. (2002) The Cambridge Structural Database: A quarter of a million crystal structures and rising. *Acta Crystallogr. B58*, 380–388.
21. Laskowski, R. A., MacArthur, M. W., Moss, D. S., and Thornton, J. M. (1993) PROCHECK: A program to check the stereochemical quality of protein structures. *J. Appl. Crystallogr. 26*, 283–291.
22. McGaughey, G. B., Gagné, M., and Rappé, A. K. (1998) π-Stacking Interactions Alive and Well in Proteins. *J. Biol. Chem. 273*, 15458–15463.
23. Henderson, J. N., and Remington, S. J. (2005) Crystal structures and mutational analysis of amFP486, a cyan fluorescent protein from *Anemonia majano*. *Proc. Natl. Acad. Sci. U.S.A. 102*, 12712–12717.
24. Burghardt, T. P., Juranić, N., Macura, S., and Ajtai, K. (2002) Cation-π interaction in a folded polypeptide. *Biopolymers 63*, 261–272.
25. Sniegowski, J. A., Phail, M. E., and Wachter, R. M. (2005) Maturation efficiency, trypsin sensitivity, and optical properties of Arg96, Glu222 and Gly67 variants of green fluorescent protein. *Biochem. Biophys. Res. Commun. 332*, 657–663.
26. Wood, T. I., Barondeau, D. P., Hitomi, C., Kassmann, C. J., Tainer, J. A., and Getzoff, E. D. (2005) Defining the role of arginine 96 in green fluorescent protein fluorophore biosysthesis. *Biochemistry 44*, 16211–16220.
27. Remington, S. J. (2006) Fluorescent proteins: Maturation, photochemistry and photophysics. *Curr. Opin. Struct. Biol. 16*, 714–721.
28. Bae, J. H., Rubini, M., Jung, G., Wiegand, G., Seifert, M. H. J., Azim, M. K., Kim, J. S., Zumbusch, A., Holak, T. A., Moroder, L., Huber, R., and Budisa, N. (2003) Expansion of the genetic code enables design of a novel "Gold" class of green fluorescent proteins. *J. Mol. Biol. 328*, 1071–1081.

BI800727V